

Analysis and synthesis of feature map for kernel-based quantum classifier

Yudai Suzuki · Hiroshi Yano · Qi Gao · Shumpei Uno · Tomoki Tanaka · Manato Akiyama · Naoki Yamamoto

Received: date / Accepted: date

Abstract A method for analyzing and synthesizing the feature map for the kernel-based quantum classifier is developed, using the Pauli decomposition. In particular, for 2-dimensional input datasets, the method boils down to a general formula that easily computes a lower bound of the exact training accuracy, which eventually helps us to see whether the selected feature map is suitable for linearly separating the dataset. Also, a synthesis method, that combines different kernels to construct a better-performing feature map in a larger feature space, is demonstrated.

Y. Suzuki, H. Yano: Equally contributing authors.

Yudai Suzuki
Department of Mechanical Engineering, Keio University, Hiyoshi 3-14-1, Kohoku, Yokohama 223-8522, Japan

Hiroshi Yano
Department of Information and Computer Science, Keio University, Hiyoshi 3-14-1, Kohoku, Yokohama 223-8522, Japan

Qi Gao · Shumpei Uno · Tomoki Tanaka · Naoki Yamamoto
Quantum Computing Center, Keio University, Hiyoshi 3-14-1, Kohoku, Yokohama 223-8522, Japan

Manato Akiyama
Department of Biosciences and Informatics, Keio University, Hiyoshi 3-14-1, Kohoku, Yokohama 223-8522, Japan

Qi Gao
Mitsubishi Chemical Corporation Science & Innovation Center, 1000, Kamoshida-cho, Aoba-ku, Yokohama 227-8502, Japan

Shumpei Uno
Mizuho Information & Research Institute, Inc., 2-3 Kanda-Nishikicho, Chiyoda-ku, Tokyo 101-8443, Japan

Tomoki Tanaka
Mitsubishi UFJ Financial Group, Inc. and MUFG Bank, Ltd., 2-7-1 Marunouchi, Chiyoda-ku, Tokyo 100-8388, Japan

Naoki Yamamoto
Department of Applied Physics and Physico-Informatics, Keio University, Hiyoshi 3-14-1, Kohoku, Yokohama 223-8522, Japan, E-mail: yamamoto@appi.keio.ac.jp

1 Introduction

Over the last 20 years, the unprecedented improvements in the cost-effectiveness ratio of computer, together with improved computational techniques, make machine learning widely applicable in every aspect of our lives such as education, healthcare, games, finance, transportation, energy, business, science and engineering [1, 2]. Among numerous developed machine learning methods, Support Vector Machine (SVM) is a very established one which has become an overwhelmingly popular choice for data analysis [3]. In SVM method, a nonlinear dataset is transformed via a feature map to another dataset and is separated by a hyperplane in the feature space, which can be effectively performed using the kernel trick. In particular, the Gaussian kernel is often used.

Quantum computing is expected to speed-up the performance of machine learning through exploiting quantum mechanical properties including superposition, interference, and entanglement. As for the quantum classifier, a renaissance began in the past few years, with the quantum SVM method [4], the quantum circuit learning method [5], and some parallel development by other research groups [6,7]. In particular, the kernel method can be exploited as a powerful mean that can be introduced in the quantum SVM as in the classical case [4, 8–14]; importantly, the concept of kernel-based quantum classifier has been experimentally demonstrated on a real device [11, 14]. These studies show the possibility that machine learning will get a further boost by using quantum computers in the near future.

For all the developed quantum classification methods, the feature map plays a role to encode the dataset taken from its original low dimensional real space onto a high dimensional quantum state space (i.e., Hilbert space). The possible advantage of quantum classifier lies in the fact that this high-dimensional feature space is realized on a physical quantum

computer even with a medium number of qubits, as well as the fact that the kernel can be computed faster than the classical case. However, unlike the classical case, to fully exploit the quantum nature, the feature map has to be explicitly specified (that is, the kernel trick cannot be applied). Choosing a suitable feature map, which may presumably achieve a high training accuracy, is of course a non-trivial task; one can prepare many feature map candidates and try to find a suitable one by comparing the results of training accuracy attained with all those feature maps, but this clearly needs numerous times of classification or regression analysis. Hence it would be desirable if we have a method for easily having a rough estimate of the training accuracy of every feature map candidate, which further enables us to synthesize a well-performing feature map.

Towards this goal, this paper proposes a method that, based on the real-vector representation of the mapped quantum state via the Pauli decomposition of the corresponding density matrix, gives us a visualization of the encoded input data distribution and, further, enables us to easily calculate the *minimum accuracy*, i.e., a lower bound of the exact training accuracy, without performing the actual classification procedure. The minimum accuracies calculated for the feature map candidates can be used to screen a library of suitable feature maps. Moreover, the visualized feature map candidates might be exploited for combining them to construct a better-performing feature map and accordingly a better kernel. Although the concept of these synthesizing tools is device-independent, in this paper we demonstrate the idea in the framework of [11], with a special type of five feature maps and four 2-dimensional nonlinear datasets.

2 Methods

2.1 Real-vector representation of the feature map via Pauli decomposition

In the SVM method with quantum kernel estimator, the feature map transforms an input dataset to a set of multi-qubit states, which forms the feature space (i.e., Hilbert space); then the kernel matrix is constructed by calculating all the inner products of quantum states, and it is finally used in the (standard) SVM for classifying the dataset. Surely different feature maps lead to different kernels and accordingly influence a lot on the classification accuracy, meaning that a careful analysis of the feature space is necessary. However, due to the complicated structure of the feature space, such analysis is in general not straightforward. Here we propose the Pauli-decomposition-based method for visualizing the feature space, which might be used as a guide to select a suitable feature map.

Here we give a brief summary of the kernel-based quantum SVM method proposed in [11]. First, a classical data

$\mathbf{x} \in \mathbb{R}^n$ is encoded into the unitary operator $\mathcal{U}_{\Phi(\mathbf{x})}$ through an *encoding function* $\Phi(\mathbf{x})$, and it is applied to the initial state $|0\rangle^{\otimes n}$ with $|0\rangle$ the qubit ground state; note that we here assume that the number of qubits is equal to the dimension of the classical data (or more precisely the number of feature variables of the data). Thus, the feature map is a transformation from the classical data \mathbf{x} to the quantum state $|\Phi(\mathbf{x})\rangle = \mathcal{U}_{\Phi(\mathbf{x})}|0\rangle^{\otimes n}$, and the feature space is $(\mathbb{C}^2)^{\otimes n} = \mathbb{C}^{2^n}$. The kernel is then naturally defined as $K(\mathbf{x}, \mathbf{z}) = |\langle \Phi(\mathbf{x}) | \Phi(\mathbf{z}) \rangle|^2$; this quantity can be practically calculated as the ratio of zero strings 0^n in the Z -basis measurement result, for the state $\mathcal{U}_{\Phi(\mathbf{x})}^\dagger \mathcal{U}_{\Phi(\mathbf{z})} |0\rangle^{\otimes n}$. Finally, the constructed kernel is used in the standard manner in SVM; that is, a test data \mathbf{x} is classified into two categories depending on the sign of

$$\sum_{i=1}^N \alpha_i y_i K(\mathbf{x}_i, \mathbf{x}) + b, \quad (1)$$

where (\mathbf{x}_i, y_i) ($i = 1, \dots, N$) is the pair of training data, and (α_i, b) are the optimized parameters. A possible advantage in using the quantum system for the classification problem would lie in the fact that even an intermediate-scale quantum computer with e.g. $n = 20$ has a huge dimensional feature space of dimension $2^{20} \approx 1,000,000$.

Now we introduce the real-vector representation of the feature map. The key idea is simply to use the fact that the kernel can be expressed in terms of the density operator $\rho(\mathbf{x}) = |\Phi(\mathbf{x})\rangle \langle \Phi(\mathbf{x})|$ as

$$K(\mathbf{x}, \mathbf{z}) = |\langle \Phi(\mathbf{x}) | \Phi(\mathbf{z}) \rangle|^2 = \text{tr}[\rho(\mathbf{x})\rho(\mathbf{z})], \quad (2)$$

and the density operator can be always expanded by the set of Pauli operators as

$$\rho(\mathbf{x}) = \sum_{i=1}^{4^n} a_i(\mathbf{x}) \sigma_i \quad (3)$$

with $a_i(\mathbf{x}) \in \mathbb{R}$ and $\sigma_i \in P_n = \{I, X, Y, Z\}^{\otimes n}$ the multi-qubit Pauli operators. The followings are examples of the elements of P_2 :

$$XI = \begin{bmatrix} 0 & 1 \\ 1 & 0 \end{bmatrix} \otimes \begin{bmatrix} 1 & 0 \\ 0 & 1 \end{bmatrix}, \quad ZY = \begin{bmatrix} 1 & 0 \\ 0 & -1 \end{bmatrix} \otimes \begin{bmatrix} 0 & -i \\ i & 0 \end{bmatrix},$$

$$YZ = \begin{bmatrix} 0 & -i \\ i & 0 \end{bmatrix} \otimes \begin{bmatrix} 1 & 0 \\ 0 & -1 \end{bmatrix}.$$

Then, by substituting Eq. (3) into Eq. (2) and using the trace relation $\text{tr}(\sigma_i \sigma_j) = 2^n \delta_{i,j}$, the kernel can be written as

$$K(\mathbf{x}, \mathbf{z}) = 2^n \sum_{i=1}^{4^n} a_i(\mathbf{x}) a_i(\mathbf{z}), \quad (4)$$

meaning that the vector $\mathbf{a}(\mathbf{x}) = [a_1(\mathbf{x}), \dots, a_{4^n}(\mathbf{x})]^\top$ serves as the feature map corresponding to the kernel $K(\mathbf{x}, \mathbf{z})$. That is, the input dataset $\{\mathbf{x}_i\}$ are encoded into the set of vectors

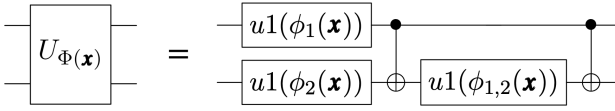


Fig. 1 Quantum circuit of $U_{\Phi(\mathbf{x})}$ with the encoding function $\Phi(\mathbf{x}) = \{\phi_1(\mathbf{x}), \phi_2(\mathbf{x}), \phi_{1,2}(\mathbf{x})\}$, composed of the three phase-shift gates of the form $u1(\phi) = \text{diag}\{1, e^{-i\phi}\}$ and two Controlled-NOT gates.

$\{\mathbf{a}(\mathbf{x}_i)\}$ in a much-bigger *real* feature space \mathbb{R}^{4^n} and will be classified by the SVM with the kernel (4).

Note that $\mathbf{a}(\mathbf{x})$ is a generalization of the Bloch vector, and thus the corresponding feature space is interpreted as the generalized Bloch sphere. Also thanks to the real-valued representation of the feature map, one can calculate the *VC dimension*; from the theory for the family of classifiers using SVM [15], the VC dimension in our case is $4^n + 1$. In general, the VC dimension represents a measure of the capacity of the feature space and can be used to estimate the upper bound of the generalization error.

2.2 Feature map for 2-dimensional input data

In this paper we study the case of two-dimensional input data $\mathbf{x} \in \mathbb{R}^2$ and particularly follow the procedure of [11]; in the case $n = 2$, an input data \mathbf{x} is mapped to the unitary operator $\mathcal{U}_{\Phi(\mathbf{x})}$ through the set of encoding functions $\Phi(\mathbf{x}) = \{\phi_1(\mathbf{x}), \phi_2(\mathbf{x}), \phi_{1,2}(\mathbf{x})\}$, which is composed of two layers of Hadamard gate $H^{\otimes 2}$ and the unitary gate $U_{\Phi(\mathbf{x})}$ as follows:

$$\mathcal{U}_{\Phi(\mathbf{x})} = U_{\Phi(\mathbf{x})} H^{\otimes 2} U_{\Phi(\mathbf{x})} H^{\otimes 2}, \quad (5)$$

where

$$U_{\Phi(\mathbf{x})} = \exp\left(i\phi_1(\mathbf{x})ZI + i\phi_2(\mathbf{x})IZ + i\phi_{1,2}(\mathbf{x})ZZ\right). \quad (6)$$

The quantum circuit representation realizing this unitary gate is shown in Fig. 1. The three user-defined encoding functions $\phi_1(\mathbf{x}), \phi_2(\mathbf{x})$, and $\phi_{1,2}(\mathbf{x})$ nonlinearly transform the input data \mathbf{x} into the qubit $|\Phi(\mathbf{x})\rangle = \mathcal{U}_{\Phi(\mathbf{x})}|0\rangle^{\otimes 2}$. Now, through a lengthy calculation, we have the explicit Pauli decomposed form (3) of the density operator $\rho(\mathbf{x}) = |\Phi(\mathbf{x})\rangle\langle\Phi(\mathbf{x})|$; the coefficients $\{a_i(\mathbf{x})\}$ with $i = II, XI, YI, \dots, ZZ$ are listed in Table 1. The coefficients are composed of bunch of trigonometric functions, which make the kernel complicated enough to transform the input data highly nonlinearly.

2.3 Minimum accuracy

Here we give the definition of the minimum accuracy and explain how to calculate it. First, for a fixed index i and the training dataset $\{\mathbf{x}_k, y_k\}_{k=1, \dots, N}$, we calculate the i th-axis accuracy R_i through the following procedure: (i) for a fixed

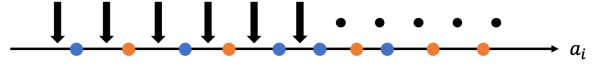


Fig. 2 Example of the procedure for calculating the i th-axis accuracy R_i for the 1-dimensional data $\{a_i(\mathbf{x}_k)\}_{k=1, \dots, N}$. The orange or blue point indicates the value of y_k . The accuracy with fixed threshold is defined as $(\max\{n_b, n_o\} + N - \min\{n_b, n_o\}) / 2n$ where n_b and n_o are the number of blue and orange points in the left side of the threshold, respectively. For example, for the third threshold from the left, the accuracy is 0.5. Changing the threshold, we find that the maximum of these values is $R_i = 0.7$.

threshold between a pair of two neighboring data points, indicated by an arrow shown in Fig. 2, calculate the accuracy of this simple classification task via this threshold on the 1-dimensional dataset $\{a_i(\mathbf{x}_k)\}_{k=1, \dots, N}$, (ii) calculate the accuracies for all the thresholds, and finally (iii) determine the i th-axis accuracy R_i as the maximum of these values. An example is given in the caption of Fig. 2. Then, the minimum accuracy is defined as $\max_i R_i$, where the index takes $i = II, XI, YI, \dots, ZZ$ for the case $n = 2$. Importantly, this procedure for obtaining the minimum accuracy can be readily done, because the data points are directly produced from the functions $\{a_i(\mathbf{x})\}$ listed in Table 1, and each classification task needs neither a kernel matrix nor the SVM optimization procedure but it is merely a line search. Also note that R_i represents the success rate of classification via the hyperplane orthogonal to the i th axis; in view of the fact that the optimal hyperplane in the feature space, which best classifies the dataset, is in general orthogonal to none of the basis axis, the minimum accuracy $\max_i R_i$ gives a lower bound of the exact training accuracy achieved by the SVM. Hence, the minimum accuracy can be used as a convenient measure for estimating the worst-case accuracy and eventually a guide of selecting a suitable encoding function and accordingly a suitable feature map.

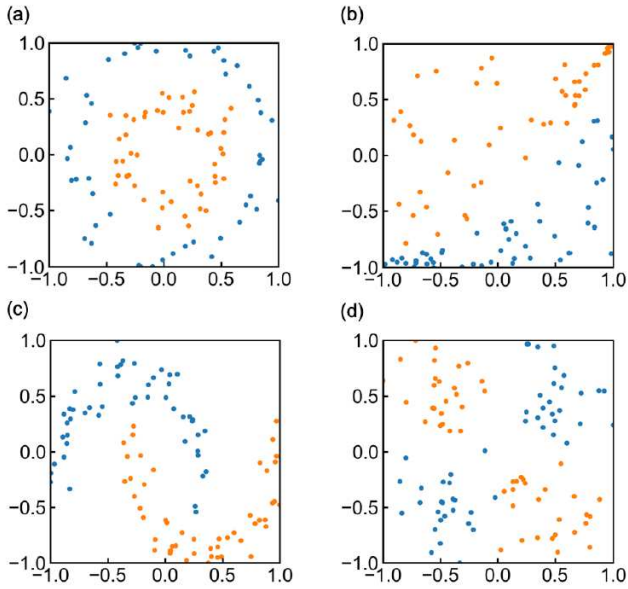
3 Results and Discussions

3.1 Classification accuracy with different encoding functions

Here we apply the quantum SVM method, with several encoding functions, to the benchmark classification problems. We consider the nonlinear 2-dimensional datasets, Circle, Exp, Moon, and Xor, shown in Fig. 3; in each case, 100 data points are generated and categorized to two groups (orange or blue). Each dataset is encoded into the two-qubits quan-

Table 1 Pauli decomposition coefficients for 2-dimensional input data, $\{a_i(\mathbf{x})\}$ with $i = II, XI, YI, \dots, ZZ$.

Index i	Pauli decomposition coefficients a_i
II	$1/4$
XI	$\{\sin \phi_1 (\sin \phi_2 \sin \phi_{1,2}^2 + \sin \phi_1 \cos \phi_{1,2}^2 + \cos \phi_2 \cos \phi_1 \sin \phi_{1,2})\}/4$
YI	$\{-\sin \phi_2 \cos \phi_1 \sin \phi_{1,2}^2 - \sin \phi_1 \cos \phi_1 \cos \phi_{1,2}^2 + \cos \phi_2 \sin \phi_1^2 \sin \phi_{1,2}\}/4$
ZI	$\cos \phi_1 \cos \phi_{1,2}/4$
IX	$\{\sin \phi_2 (\sin \phi_1 \sin \phi_{1,2}^2 + \sin \phi_2 \cos \phi_{1,2}^2 + \cos \phi_1 \cos \phi_2 \sin \phi_{1,2})\}/4$
XX	$\{\sin \phi_1^2 \sin \phi_2^2 + \sin \phi_{1,2} \cos \phi_1 \cos \phi_2 (\sin \phi_1 + \sin \phi_2)\}/4$
YX	$\{-\sin \phi_2^2 \sin \phi_1 \cos \phi_1 + \sin \phi_{1,2} \cos \phi_2 (\sin \phi_1 \sin \phi_2 - \cos \phi_1^2)\}/4$
ZX	$\{\cos \phi_{1,2} (-\sin \phi_1 \cos \phi_2 \sin \phi_{1,2} + \cos \phi_1 \sin \phi_2^2 + \sin \phi_2 \cos \phi_2 \sin \phi_{1,2})\}/4$
IY	$\{-\sin \phi_1 \cos \phi_2 \sin \phi_{1,2}^2 - \sin \phi_2 \cos \phi_2 \cos \phi_{1,2}^2 + \cos \phi_1 \sin \phi_2^2 \sin \phi_{1,2}\}/4$
XY	$\{-\sin \phi_1^2 \sin \phi_2 \cos \phi_2 + \sin \phi_{1,2} \cos \phi_1 (\sin \phi_1 \sin \phi_2 - \cos \phi_2^2)\}/4$
YY	$\{\sin \phi_1 \cos \phi_1 \sin \phi_2 \cos \phi_2 - \sin \phi_{1,2} (\cos \phi_2^2 \sin \phi_1 + \sin \phi_2 \cos \phi_1^2)\}/4$
ZY	$\{\sin \phi_2 (-\sin \phi_1 \sin \phi_{1,2} \cos \phi_{1,2} - \cos \phi_2 \cos \phi_1 \cos \phi_{1,2} + \sin \phi_2 \cos \phi_{1,2} \sin \phi_{1,2})\}/4$
IZ	$\cos \phi_2 \cos \phi_{1,2}/4$
XZ	$\{\cos \phi_{1,2} (-\sin \phi_2 \cos \phi_1 \sin \phi_{1,2} + \cos \phi_2 \sin \phi_1^2 + \sin \phi_1 \cos \phi_1 \sin \phi_{1,2})\}/4$
YZ	$\{\sin \phi_1 (-\sin \phi_2 \sin \phi_{1,2} \cos \phi_{1,2} - \cos \phi_1 \cos \phi_2 \cos \phi_{1,2} + \sin \phi_1 \cos \phi_{1,2} \sin \phi_{1,2})\}/4$
ZZ	$\cos \phi_1 \cos \phi_2/4$

**Fig. 3** Dataset called (a) Circle, (b) Exp, (c) Moon, and (d) Xor.

tum state, with the following five encoding functions:

$$\phi_1(\mathbf{x}) = x_1, \phi_2(\mathbf{x}) = x_2, \phi_{1,2}(\mathbf{x}) = \pi x_1 x_2, \quad (7)$$

$$\phi_1(\mathbf{x}) = x_1, \phi_2(\mathbf{x}) = x_2, \phi_{1,2}(\mathbf{x}) = \frac{\pi}{2}(1 - x_1)(1 - x_2), \quad (8)$$

$$\phi_1(\mathbf{x}) = x_1, \phi_2(\mathbf{x}) = x_2, \phi_{1,2}(\mathbf{x}) = \exp\left(\frac{|x_1 - x_2|^2}{8/\ln(\pi)}\right), \quad (9)$$

$$\phi_1(\mathbf{x}) = x_1, \phi_2(\mathbf{x}) = x_2, \phi_{1,2}(\mathbf{x}) = \frac{\pi}{3 \cos(x_1) \cos(x_2)}, \quad (10)$$

$$\phi_1(\mathbf{x}) = x_1, \phi_2(\mathbf{x}) = x_2, \phi_{1,2}(\mathbf{x}) = \pi \cos(x_1) \cos(x_2). \quad (11)$$

The functions $\phi_{1,2}(\mathbf{x})$ are chosen from a set of various non-linear functions in the range of 2π , i.e. $\max(\phi) - \min(\phi) \leq 2\pi$ for $x_1, x_2 \in [-1, 1]$. In particular, the coefficient of (9) and (10) are determined empirically so that the resulting classifier achieves a high accuracy on the prepared datasets. Also

the reason of fixing $\phi_1(\mathbf{x}) = x_1$ and $\phi_2(\mathbf{x}) = x_2$ for all the encoding functions is that here we aim to investigate the dependence of the classification accuracy on $\phi_{1,2}(\mathbf{x})$. In this work, the classification accuracy are evaluated as the average accuracy of the 5-fold cross validation, where one dataset is divided into 5 groups with equal number of datasets (i.e., 20 data-points), for both the training and test dataset. All the calculations are carried out using QASM simulator included in the Qiskit package [16]. The number of shot is 10,000, which is used to construct the estimate of the kernel.

The classification accuracy of the four dataset, achieved by the above different encoding functions, are shown in Table 2(a) for the training case and Table 2(b) for the test case. For all the cases, (8) achieves the best accuracy larger than 0.96 for the training set and 0.91 for the test set. This result means that (8) is recommended to use for constructing the suitable feature map. On the other hand, the accuracy of dataset calculated using (7) and (9) is not always good. For example, (7) achieves the accuracy 1.00 and 0.96 for the training dataset of Circle and Xor, respectively, whereas the accuracy for the training Exp and Moon datasets are decreased to 0.88 and 0.86, respectively. Similar results are also observed for the case of (9). These facts clearly show that the different encoding functions, which lead to the different feature maps and kernels, largely influence the resulting classification accuracy.

3.2 Analysis of the feature map in the real-vector representation

We now apply our method to the classification problem described above, and see how the new feature map $\mathbf{a}(\mathbf{x})$ would benefit us to figure out the distribution of dataset in the feature space, and moreover, enable us to predict a suitable encoding function using the minimum accuracy.

Table 2 Classification accuracy achieved by the quantum SVM method, for 4 nonlinear datasets and five different encoding functions.

(a) Training accuracy				
encoding function	Circle	Exp	Moon	Xor
(7)	1.00	0.88	0.86	0.96
(8)	0.99	0.96	0.98	0.97
(9)	1.00	0.98	0.85	0.99
(10)	1.00	0.91	0.93	0.99
(11)	1.00	0.98	0.97	0.93

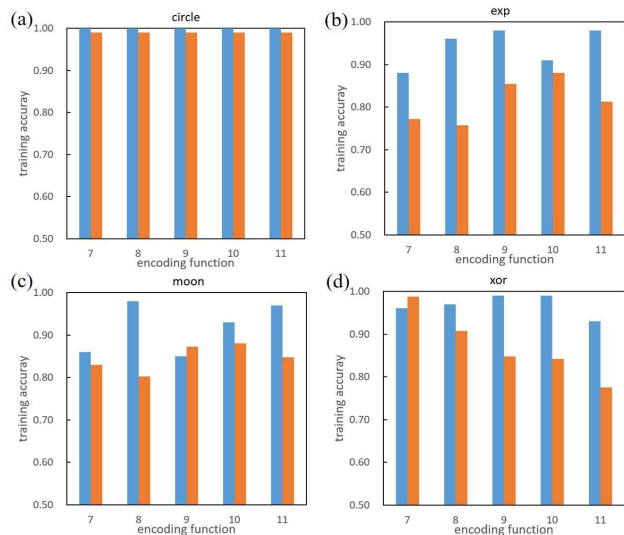
(b) Test accuracy				
encoding function	Circle	Exp	Moon	Xor
(7)	0.99	0.89	0.84	0.96
(8)	0.95	0.93	0.91	0.93
(9)	1.00	0.97	0.80	0.97
(10)	1.00	0.90	0.93	0.99
(11)	1.00	0.96	0.91	0.90

First, Figs. 6-10 show the color map of $a_i(\mathbf{x})$ as a function of $\mathbf{x} \in \mathbb{R}^2$ with $i = II, XI, YI, \dots, ZZ$ for the encoding functions (7)-(11), respectively. Note that each $a_i(\mathbf{x})$ is not determined from a specific input dataset. Nevertheless, very interestingly, some of those 2-dimensional spaces intrinsically possess the shape of distribution of the coming input dataset, which will thus affect on the resulting classification accuracy. For example, in all cases of Figs. 6-10 the ZZ element $a_{ZZ}(\mathbf{x})$ has a circle shape, meaning that Circle dataset can be classified only by the feature map $a_{ZZ}(\mathbf{x})$; this observation is consistent with the fact that Circle dataset can be indeed classified with high training/test accuracies as shown in Tables 2(a) and 2(b). Similar results can also be clearly found in Fig. 6 (the case of encoding function (7)) and in Fig. 8 (the case of (9)); the shape of $a_{YX}(\mathbf{x})$ in Fig. 6 has a similar distribution to Xor dataset, and actually (7) achieves the high training accuracy 0.96 for Xor dataset; the shape of $a_{ZX}(\mathbf{x})$ in Fig. 8 has a similar distribution to Exp dataset, and actually (9) achieves the high training accuracy 0.98 for Exp dataset.

Next, Table 3 gives the minimum accuracy for the encoding functions (7)-(11), which are calculated according to the procedure given in Section 2.3. Recall that the minimum accuracy gives a lower bound of the exact training accuracy, or equivalently, guarantees a worst-case accuracy. Hence, our suggestion is to select the encoding function that has the largest minimum accuracy; that is, for Exp dataset, the encoding function (10) is recommended to use; similarly, for Moon and Xor datasets, (10) and (7) are recommended, respectively. Also for the case of Circle dataset, any encoding function can be used. Now let us compare the minimum accuracy with the exact training accuracies given in Table 2(a). Figure 4 gives the summary, where the minimum and exact accuracies are indicated with the orange and blue bars, respectively. Importantly, the encoding function selected according to the above-mentioned guide based on the minimum accuracy, does not necessarily produce the best train-

Table 3 The minimum accuracy calculated using the Pauli decomposition coefficients shown in Figs. 6-10.

encoding function	circle	exp	moon	xor
(7)	0.99	0.77	0.83	0.99
(8)	0.99	0.76	0.80	0.91
(9)	0.99	0.86	0.87	0.85
(10)	0.99	0.88	0.88	0.84
(11)	0.99	0.81	0.85	0.78

**Fig. 4** Comparison between the exact training accuracy in Table 2(a) (blue) and the minimum accuracy in Table 3 (orange).

ing accuracies. Nonetheless, for all the cases of dataset, the selected encoding functions achieve the training accuracies bigger than 0.9. Therefore, in light of the fact that the minimum accuracy is obtained immediately without calculating the kernel matrix nor performing the SVM optimization procedure, our conclusion is that the minimum accuracy can be used as a convenient measure for determining a suitable encoding function and accordingly a good feature map. Finally note that, as seen in Fig. 4 (c), (d), the encoding functions (9) for Moon and (7) for Xor do not give a lower bound, due to the statistical errors; this gap can be decreased by taking more sample points.

3.3 Synthesis of the feature map via the combined Kernel method: Toward ensemble learning

In the classical regime there have been a number of works on designing efficient kernels; a simple strategy is to combine some different kernels to construct a single kernel, so that the constructed one might have a desired characteristic by compensating the weakness of each kernel [17]. Here we demonstrate that this idea works in quantum regime as well, as actually in the above sections we have introduced several types of encoding functions which indeed lead to different

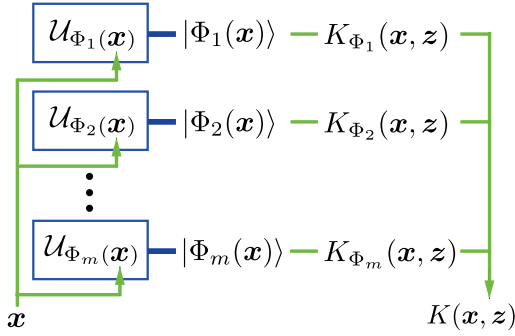


Fig. 5 Scheme of the kernel synthesizer composed of different (weak) quantum computers.

kernel functions and accordingly different classification performances. Note that the idea of combined kernel for quantum classifier was briefly addressed in [8] yet without concrete demonstration.

A typical combining method of kernels is to take a summation of them, as illustrated in Fig. 5:

$$K(\mathbf{x}, \mathbf{z}) = \sum_{i=1}^m \lambda_i K_{\Phi_i}(\mathbf{x}, \mathbf{z}),$$

where λ_i are the weighting parameters satisfying $\sum_{i=1}^m \lambda_i = m$ with $0 \leq \lambda_i \leq m$ (normalization of $\{\lambda_i\}$ does not lead to any essential difference). Here, to demonstrate this idea, we consider the combination of two equally-weighted kernels, i.e., the case of $m = 2$ and $\lambda_1 = \lambda_2 = 1$; see [18, 19] for the validity of this choice in the classical case. Even in this simple case a possible advantage may be readily seen; that is, a sum of kernels theoretically results in a higher dimensional feature space than that of the original ones as follows:

$$\begin{aligned} K_{\Phi_1}(\mathbf{x}, \mathbf{z}) + K_{\Phi_2}(\mathbf{x}, \mathbf{z}) &= |\langle \Phi_1(\mathbf{x}) | \Phi_1(\mathbf{z}) \rangle|^2 + |\langle \Phi_2(\mathbf{x}) | \Phi_2(\mathbf{z}) \rangle|^2 \\ &= |\langle \Phi_1 \oplus \Phi_2(\mathbf{x}) | \Phi_1 \oplus \Phi_2(\mathbf{z}) \rangle|^2, \end{aligned}$$

where $|\Phi_1 \oplus \Phi_2(\mathbf{x})\rangle = |\Phi_1(\mathbf{x})\rangle \oplus |\Phi_2(\mathbf{x})\rangle$, meaning that the classical data $\mathbf{x} \in \mathbb{R}^n$ is encoded into the direct sum of two Hilbert spaces and hence the dimension of the feature space is doubled. Here we consider the same benchmark classification problems as above, by applying the two-qubits ($n = 2$) classifier with the kernel constructed from the encoding functions (7) and (9). In this case $\mathbf{a}(\mathbf{x})$ is a 32 dimensional real vector, but with two redundant elements a_{II} and a_{ZZ} .

We first test the kernel using the encoding function (9) combined with the other four, and see how much it may improve the classification accuracy for Moon dataset for which the classifier using the single encoding function (9) showed the worst training accuracy 0.85. The resultant classification accuracies obtained by applying the combined kernels are shown in Table 4(a); every kernel results in improving the classification accuracy. Especially, when combining the weak classifiers with the kernels (7) and (9), in which case the training accuracy is 0.86 and 0.85 respectively, then the

Table 4 Training and Test accuracies via the classifier with combined kernels.

(a) Classification accuracies for Moon dataset				
Encoding function	(9) + (7)	(9) + (8)	(9) + (10)	(9) + (11)
Training	0.96	0.99	0.97	0.97
Test	0.92	0.93	0.93	0.92
(b) Classification accuracies for Exp dataset				
Encoding function	(7) + (8)	(7) + (9)	(7) + (10)	(7) + (11)
Training	0.95	0.96	0.98	0.98
Test	0.91	0.94	0.97	0.96

classifier with this new constructed kernel achieves the accuracy 0.96. This would make sense, because the feature space visualized by $a_i(\mathbf{x})$ of the encoding functions (7) and (9) look very different, indicating that the advantages of each classifiers might be well synthesized to achieve better classification.

Similarly, we test four combined kernels composed of the encoding function (7) and the others, to classify Exp dataset for which the single encoding function (7) led to the worst training accuracy 0.88. The resultant classification accuracies are shown in Table 4(b). In this situation, however, some of the classification performance were not so improved compared to the results using the original encoding function. This issue might be resolved by carefully choosing the weighting parameters $\{\lambda_i\}$ when synthesizing the kernels.

A broad concept behind what we have demonstrated here is the so-called *ensemble learning* [20], which is a general and effective strategy to combine several weak classifiers to generate a single stronger classifier. Actually some quantum extension of this method have been deeply investigated in [21, 22]. In our work, each classifier is weak in the sense that their circuit depth and the number of qubits are severely limited; also the difference of weak classifiers simply comes from the difference of encoding functions, and the single stronger classifier is constructed merely by taking the summation of the corresponding kernels. Systematic strategy for synthesizing weak classifiers for producing a single stronger one is important particularly in the current status where only noisy intermediate-scale quantum devices are available.

4 Conclusion

In this paper, we proposed a method that helps us to analyze and synthesize the feature map for the kernel-based quantum classifier, based on the real-value representation of it. The minimum accuracy, which serves as a lower bound of the exact accuracy, was introduced in this framework, which might be used as a tool to effectively screen a library of feature maps suitable for classification. Also the method of combining (weak) feature maps to produce a better-performing map was demonstrated with some benchmarking classification

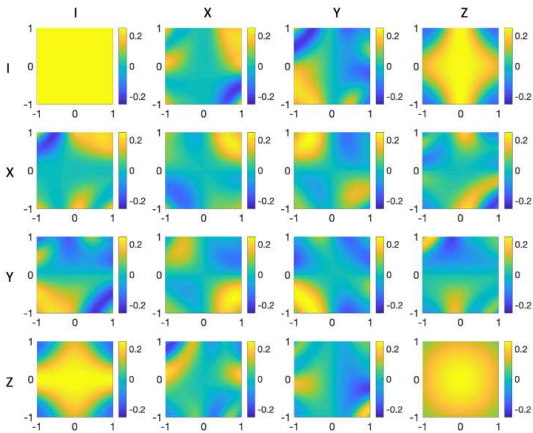


Fig. 6 Color map of all the 2-dimensional spaces $a_i(\mathbf{x})$ with the encoding function (7).

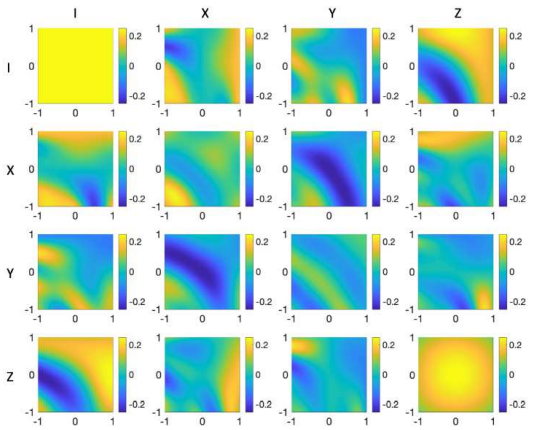


Fig. 7 Color map of all the 2-dimensional spaces $a_i(\mathbf{x})$ with the encoding function (8).

problems. It is important to extend the presented method, beyond a demonstration, to a general and systematic one for constructing a quantum classifier which fully makes use of its intrinsic power.

Acknowledgements This work was supported by MEXT Quantum Leap Flagship Program Grant Number JPMXS0118067285 and Cabinet Office PRISM.

References

1. Hastie, T., Tibshirani, R., Friedman, J.H. The elements of statistical learning: data mining, inference, and prediction, 2nd Edition. Springer series in statistics. Springer (2009)
2. Alpaydin, E.: Machine Learning: The New AI. MIT Press Essential Knowledge. MIT Press, Cambridge, MA (2016)
3. Boser, B.E., Guyon, I.M., Vapnik, V.N. : A Training Algorithm for Optimal Margin Classifiers. Proceedings of the Fifth Annual Workshop on Computational Learning Theory, **5**, pp. 144-152, (1992)

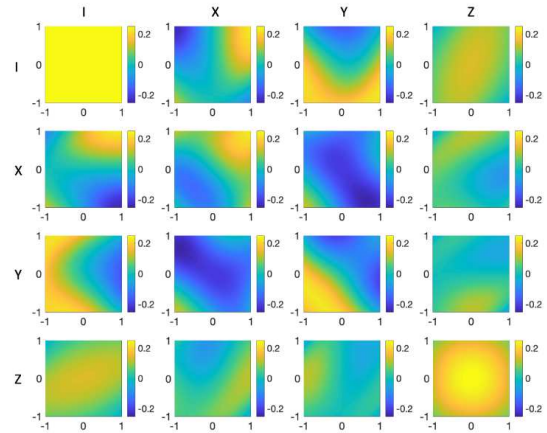


Fig. 8 Color map of all the 2-dimensional spaces $a_i(\mathbf{x})$ with the encoding function (9).

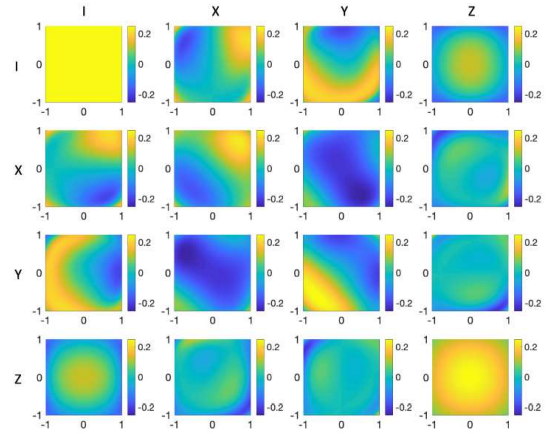


Fig. 9 Color map of all the 2-dimensional spaces $a_i(\mathbf{x})$ with the encoding function (10).

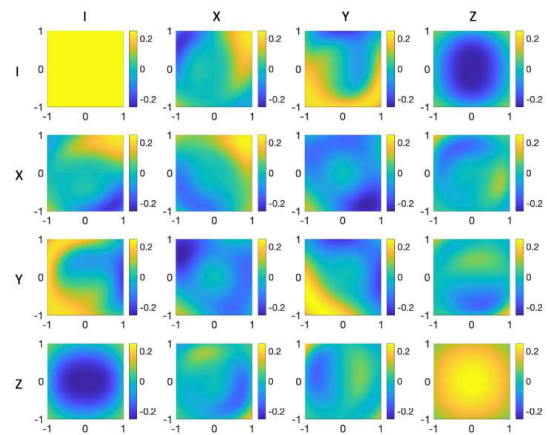


Fig. 10 Color map of all the 2-dimensional spaces $a_i(\mathbf{x})$ with the encoding function (11).

4. Reberntrost, P., Mohseni, M., Lloyd, S.: Quantum support vector machine for big data classification. *Phys. Rev. Lett.* **113**, 130503 (2014)
5. Mitarai, K., Negoro, M., Kitagawa, M., Fujii, K.: Quantum circuit learning. *Phys. Rev. A* **98**, 032309 (2018)
6. Farhi, E., Neven, H.: Classification with quantum neural networks on near term processors. arXiv:1802.06002 (2018).
7. Zhuang, Q., Zhang, Z.: Supervised learning enhanced by an entangled sensor network. arXiv:1901.09566 (2019)
8. Chatterjee, R., Yu, T.: Generalized coherent states, reproducing kernels, and quantum support vector machines. *Quantum Inf. Commun.* **17**, 1292 (2017).
9. Bishwas, A.K., Mani, A., Palade, V.: An all-pair quantum SVM approach for big data multiclass classification. *Quantum Information Processing* **17** (10), 282 (2018)
10. Li, T., Chakrabarti, S., Wu, X.: Sublinear quantum algorithms for training linear and kernel-based classifiers. In: *Proceedings of the 36th International Conference on Machine Learning (ICML 2019)*, vol. PMLR 97, pp. 3815–3824 (2019)
11. Havlíček, V., Córcoles, A.D., Temme, K., Harrow, A.W., Kandala, A., Chow, J.M., Gambetta, J.M.: Supervised learning with quantum-enhanced feature spaces. *Nature* **567** (7747), 209 (2019)
12. Schuld, M., Killoran, N.: Quantum machine learning in feature Hilbert spaces. *Phys. Rev. Lett.* **122**, 040504 (2019)
13. Bartkiewicz, K., Gneiting, C., Černoč, A., Jiráková, K., Lemr, K., Nori, F.: Experimental kernel-based quantum machine learning in finite feature space. arXiv:1906.04137v1 (2019)
14. Blank, C., Park, D. K., Rhee, J. K. K., Petruccione, F.: Quantum classifier with tailored quantum kernel. arXiv:1909.02611 (2019)
15. Burges, C. J.: A tutorial on support vector machines for pattern recognition. *Data mining and knowledge discovery* **2** (2), 121–167 (1998)
16. Aleksandrowicz, G., Alexander, T., Barkoutsos, P., Bello, L., Ben-Haim, Y., Bucher, D., Cabrera-Hernández, F.J., Carballo-Franquis, J., Chen, A., Chen, C.F., Chow, J.M., Córcoles-Gonzales, A.D., Cross, A.J., Cross, A., Cruz-Benito, J., Culver, C., González, S.D.L.P., Torre, E.D.L., Ding, D., Dumitrescu, E., Duran, I., Eendebak, P., Everitt, M., Sertage, I.F., Frisch, A., Fuhrer, A., Gambetta, J., Gago, B.G., Gomez-Mosquera, J., Greenberg, D., Hamamura, I., Havlicek, V., Hellmers, J., Herok, Ł., Horii, H., Hu, S., Imamichi, T., Itoko, T., Javadi-Abhari, A., Kanazawa, N., Karazeev, A., Krsulich, K., Liu, P., Luh, Y., Maeng, Y., Marques, M., Martín-Fernández, F.J., McClure, D.T., McKay, D., Meesala, S., Mezzacapo, A., Moll, N., Rodríguez, D.M., Nannicini, G., Nation, P., Ollitrault, P., O’Riordan, L.J., Paik, H., Pérez, J., Phan, A., Pistoia, M., Prutyayov, V., Reuter, M., Rice, J., Davila, A.R., Rudy, R.H.P., Ryu, M., Sathaye, N., Schnabel, C., Schoute, E., Setia, K., Shi, Y., Silva, A., Siraichi, Y., Sivarajah, S., Smolin, J.A., Soeken, M., Takahashi, H., Tavernelli, I., Taylor, C., Taylour, P., Trabing, K., Treinish, M., Turner, W., Vogt-Lee, D., Vuillot, C., Wildstrom, J.A., Wilson, J., Winston, E., Wood, C., Wood, S., Wörner, S., Akhalwaya, I.Y., Zoufal, C.: Qiskit: An open-source framework for quantum computing (2019)
17. Bishop, C. M.: *Pattern recognition and machine learning (information science and statistics)*. springer-Verlag New York, Inc., Secaucus, NJ, (2006)
18. Lanckriet, G. R., Cristianini, N., Bartlett, P., Ghaoui, L. E., Jordan, M. I.: Learning the kernel matrix with semidefinite programming. *Journal of Machine learning research* **5**, pp. 27–72 (2004)
19. Dioş, L., Oltean, M., Rogozan, A., Pecuchet, J. P.: Improving svm performance using a linear combination of kernels. In *International Conference on Adaptive and Natural Computing Algorithms*, pp. 218–227. Springer, Berlin, Heidelberg. (2007)
20. Dietterich, T. G.: *Ensemble methods in machine learning*. In *International workshop on multiple classifier systems*, pp. 1–15. Springer, Berlin, Heidelberg. (2000)
21. Schuld, M., Petruccione, F.: Quantum ensembles of quantum classifiers. *Scientific reports* **8** (1), 2772 (2018)
22. Wang, X., Ma, Y., Hsieh, M. H., Yung, M.: Quantum speedup in adaptive Boosting of binary classification. arXiv:1902.00869 (2019)